Mon. Not. R. Astron. Soc. , () Printed 1 February 2008 (MN LaTeX style file v2.2)

arXiv:astro-ph/0108108v2 28 Jan 2002

# Maximum Feedback and Dark Matter Profiles of Dwarf Galaxies

Oleg Y. Gnedin and HongSheng Zhao
*Institute of Astronomy, Cambridge CB3 0HA*
`ognedin@ast.cam.ac.uk, hsz@ast.cam.ac.uk`

**ABSTRACT**

The observed rotation curves of dark matter-dominated dwarf galaxies indicate low density cores, contrary to the predictions of CDM models. A possible solution of this problem involves stellar feedback. A strong baryonic wind driven by vigorous star formation can remove a large fraction of the gas, causing the dark matter to expand. Using both numerical and analytical techniques, we explore the maximum effect of the feedback with an instantaneous removal of the gaseous disk. The energy input depends on the compactness of the disk, hence the specific angular momentum of the disk. For the plausible cosmological parameters and a wide range of the disk angular momenta, the feedback is insufficient to destroy the central halo cusp, while the inner density is lowered only by a modest factor of 2 to 6. Any realistic modeling of the feedback would have even lesser impact on dark matter. We find that no star formation effect can resolve the problems of CDM cusps.

**Key words:** galaxies: dwarf — galaxies: formation — galaxies: kinematics and dynamics — dark matter

## 1 INTRODUCTION

Dwarf spheroidal galaxies are excellent systems for testing current theories of dark matter. The large mass-to-light ratios indicate that even their centers are dominated by dark matter (Mateo 1998). The velocity dispersion profile of stars and the rotation curve of gas provide clean measures of the dynamical mass at all radii. Recent observations of the gas-rich dwarfs show a nearly solid-body rotation curve, which implies a finite core inside a few hundred pc (van den Bosch et al. 2000; de Blok et al. 2001). This is in conflict with the predictions of the cold dark matter (CDM) models. Numerical simulations invariably produce a diverging, power-law density "cusp" $\rho \propto r^{-\gamma}$ with $\gamma = 1$ (Navarro, Frenk & White 1997) or $\gamma = 1.5$ (Moore et al. 1999b) within $\sim 500\,(M_{\rm vir}/10^9 M_\odot)^{1/2}$ pc (Bullock et al. 2001a).

The additional disagreements of the CDM models with observations include (1) the prediction of too many dwarf satellites within large halos (Klypin et al. 1999; Moore et al. 1999a); (2) the triaxiality of halos in conflict with the almost spherical cores of some clusters of galaxies, as inferred from gravitational lensing (Tyson et al. 1998); (3) the efficient transport of the baryon angular momentum, leading to too small disks of spiral galaxies (Navarro & Steinmetz 2000). Of these, the central cusps seem to be the most severe discrepancy. The CDM models have been very successful in matching observations on scales larger than a Mpc, but the smaller-scale problems have lead to a recent search for alternatives to CDM. The variants include warm dark matter (e.g., Bode, Ostriker & Turok 2001) and self-interacting dark matter (Spergel & Steinhardt 2000).

We examine a possible astrophysical solution to the cusp problem, the effect of star formation feedback. The energy released in supernova explosions may heat and ionize the surrounding gas. In the event of an extremely powerful burst of star formation, the heated gas may leave the dwarf galaxy in a form of fast wind (e.g., Dekel & Silk 1986). In an idealization of this problem, a significant fraction of the gas may be removed from the dwarf halo on a timescale shorter than the dynamical time. We consider the reaction of the dark matter distribution to the sudden loss of baryonic mass in the center. Supermassive black holes can also have interesting effects, somewhat different from the gas disks, and these will be discussed elsewhere.

## 2 COSMOLOGICAL CONTEXT

We explore the maximum effect of stellar feedback on the dark matter profile, assuming (1) all cool gas within the dark halo can be removed; (2) the amount of gas locked in stars is negligible; (3) the removal of gas is instantaneous.

The initial conditions for the dark matter halo and the baryonic disk are set using the cosmological concordance model with $\Omega_m = 0.35$, $\Omega_\Lambda = 0.65$, $\Omega_b\, h^2 = 0.02$ (Bahcall et al. 1999), where $h = 0.65$ is the Hubble constant in units of

© RAS

100 km $\mathrm{s}^{-1}$ $\mathrm{Mpc}^{-1}$. This gives the average baryon fraction $f_b \equiv \Omega_b/\Omega_m \approx 0.13$. Some of the baryons associated with the halo of mass $M_{\rm vir}$ will never cool and collapse towards the center, some may be heated and ionized early on and escape the shallow potential well before the starburst. But since we are interested in the maximum effect, we assume that all the associated baryons settle into a disk with the mass $M_d = f_b\, M_{\rm vir}$.

The size of the rotationally-supported disk, $r_d$, is determined by the angular momentum of the baryons (e.g., Mo, Mao & White 1998). Cosmological simulations show that dark matter halos acquire a log-normal distribution of the dimensionless angular momentum, $\lambda \equiv J|E|^{1/2}/GM_{\rm vir}^{5/2}$, with the median $\bar{\lambda} = 0.05$ and dispersion $\sigma_\lambda = 0.5$ (Barnes & Efstathiou 1987; Efstathiou et al. 1988). If the gas had the same angular momentum as the halo, the disk size would scale with $\lambda$ ($r_d \sim \lambda^2\, r_{\rm vir}$ if disk is fully self-gravitating, and $r_d \sim \lambda\, r_{\rm vir}$ in the no self-gravity case).

Initially, in isolated halos the gas is supposed to acquire the same angular momentum per unit mass as the dark matter. As a result of hierarchical merging, the distribution of dark matter can become highly non-homogeneous. Also, the cooling and fragmentation of gas into dense clouds can transfer orbital angular momentum to the dark matter via dynamical friction and direct torques (Navarro & Benz 1991). In the end, the gaseous disk may have a significantly lower value of the parameter $\lambda_b \ll \lambda$. We mimic the effect of angular momentum redistribution by considering three model disks with different $\lambda_b$.

The dark matter distribution self-consistently adjusts to the formation of the disk in the middle of the halo. This process can be described as adiabatic contraction (Blumenthal et al. 1986; Flores et al. 1993; Dalcanton et al. 1997), which we discuss at length in §3.1. Such condensation of both baryons and dark matter has a significant effect on the central density. Figure 1 demonstrates how adiabatic contraction increases the rotation curve in the inner galaxy over that predicted by cosmological simulations and intensifies the discrepancy with observations.

After the gas blowout, the final distribution of dark matter will depend on the initial disk size in the following way. If the disk was initially relatively extended ($r_d \gtrsim r_s$) the re-expansion phase is driven by the energy input, which is proportional to the binding energy of the disk, $\propto M_d/r_d$. If the disk was very compact ($r_d \ll r_s$) only the total removed mass $M_d$ affects the results. The new equilibrium profile after the removal of the entire baryonic disk must be more extended than that prior to adiabatic contraction, because any rapid expansion increases the actions of dark matter orbits. The faster the expansion, the stronger is the effect.

The energetics of gaseous winds have been studied extensively in the past (Dekel & Silk 1986; van den Bosch et al. 2000 and references therein). In general, dwarf galaxies have shallow potential wells and it is easy to create a strong wind after a few supernova explosions. We shall simply assume that the SNe ejecta energy is sufficient and is efficiently deposited into the gas, to facilitate a rapid expulsion of nearly all the initial baryons with very little locked into stars and stellar remnants.

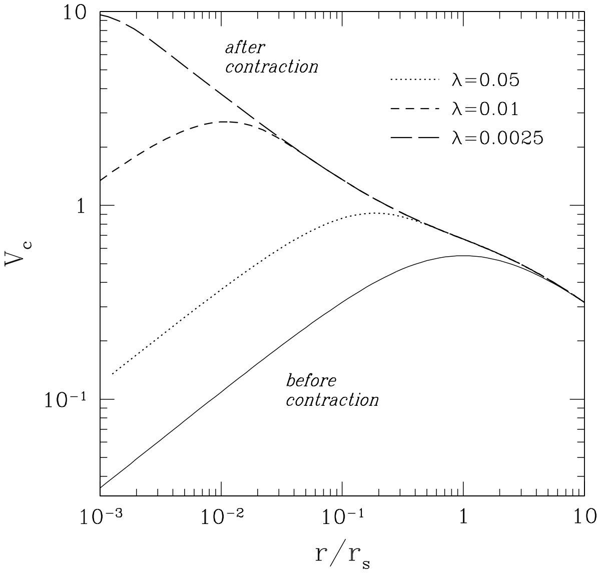

**Figure 1.** Rotation curve before and after the formation of baryonic disk and adiabatic contraction of dark matter, for three values of the angular momentum parameter, $\lambda = 0.05, 0.01, 0.0025$.

## 3 ANALYTICAL MODELS

### 3.1 Two models of adiabatic contraction

We consider the problem in a spherically-symmetric approximation. For the initial virialised halo model we use a Hernquist (1990) profile, which is a special case of a family of analytical double-power-law models (Zhao 1996) with the mass $M_{dm}(r_i)$ enclosed within radius $r_i$ given by

$$\frac{M_{dm}(r_i)}{(1-f_b)M_{\rm vir}} = \left(\frac{r_i}{r_s + r_i}\right)^{3-\gamma}, \quad \gamma = 1, \tag{1}$$

where $r_s$ is the scale radius, and $\gamma$ is the slope of the cusp. We adopt a concentration parameter $r_{\rm vir}/r_s = 10$, appropriate for the dwarf halos at high redshift, but the results at small radii are insensitive to the actual value of this parameter. The profile has the same inner slope ($\gamma = 1$) as the NFW model (Navarro, Frenk & White 1997) and deviates from it only in the outer parts which are not interesting for the present problem. The Hernquist model is more convenient both for analytical modeling and for generating the initial condition of an isolated fixed-mass halo.

During adiabatic contraction, circular orbits conserve the absolute value of the angular momentum, $GM(r)r$, and the enclosed dark matter mass, $M_{dm}(r)$. An orbit can be labeled interchangeably by its initial radius $r_i$ or by the specific angular momentum $j$, where $j$ and $r_i$ are related by

$$j^2 = r_i G M_{dm}(r_i)(1-f_b)^{-1}. \tag{2}$$

Here we use the constant factor $(1-f_b)^{-1}$ to include the mass of baryons assumed to have the same initial distribution. The orbit with an angular momentum $j$ has a post-contraction radius $r_j$ given by

$$r_j = \frac{j^2}{GM_{dm}(r_i) + GM_b(r_j)}, \tag{3}$$

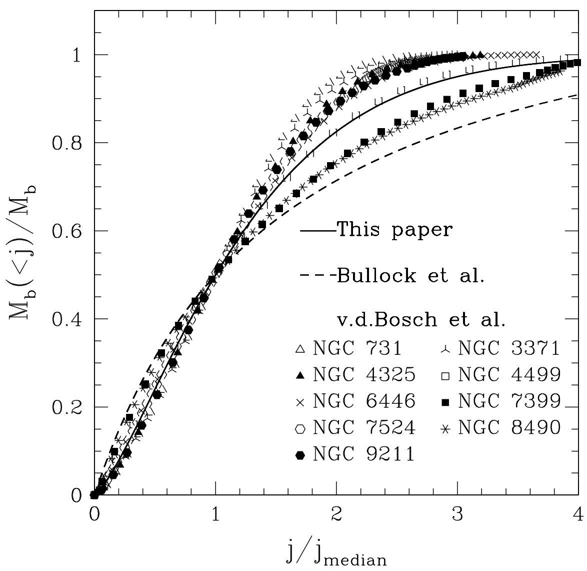

**Figure 2.** Baryon mass profile according to our angular momentum prescription (solid line, cf eq. 5 with $\gamma = 1$ and $n = 4/3$), in comparison with the universal profile (dashed line) and the observed disk galaxies (symbols), where $j_{\rm median}$ is defined such that 50% of the disk mass has the specific angular momentum $j < j_{\rm median}$. The observed disk profiles are adopted from van den Bosch, Burkert & Swaters (2001) with the stellar mass-to-light ratio $M/L_R = 1\,M_\odot/L_{R,\odot}$.

where $M_b(r_j)$ is the mass of baryons enclosed within the contracted orbit, which we need to specify separately.

We will use two independent models to evaluate adiabatic contraction.

1) Using the observations of disk galaxies as a guide, it is common to assume that the disk would have an exponential surface density profile. The enclosed disk mass is

$$M_{b,\exp}(r_j) = f_b M_{\rm vir}\left[1-(1+y)\exp(-y)\right], \qquad y \equiv \frac{r_j}{r_d}, \quad (4)$$

where the scale length $r_d$ is computed numerically by matching the total angular momentum (e.g., Mo, Mao & White 1998, their eq. 28). In this approach, $r_j$ is an implicit function of $r_i$ or $j$, and the equation must be solved iteratively.

2) Here we also take another approach, assuming the disk mass $M_b(r_j)$ can be expressed as a function $M_b(< j(r_i))$ of the initial specific angular momentum $j(r_i)$, where $j(r_i)$ is given by equation (2). The advantage is that the r.h.s. of equation (3) can now be expressed as an explicit function of $r_i$, and hence $r_j$ is computed directly without iteration as in the previous approach.

Since the $z$-component of the specific angular momentum originated from tidal torquing of neighbouring halos, hence it was distributed in the same way in baryons and dark matter, we could adopt the so-called universal angular momentum profile, $M_b(< j) = f_b M_{\rm vir}\, j/(0.8j+0.2j_{\max})$, seen in dissipationless N-body simulations of ΛCDM models (Bullock et al. 2001b), where $j_{\max}$ is the maximum specific angular momentum determined by the spin parameter $\lambda$. Unfortunately, if baryons with such a distribution collapse to a disk conserving angular momentum, then the central density of the disk would be too high and the scale length too low compared to the observed disks (Bullock et al. 2001b; van den Bosch, Burkert & Swaters 2001). The angular momentum distribution of such a disk is also very different from that of exponential disks, as shown in Fig. 2. This mismatch between the present day exponential disks and the simulated initial baryon angular momentum distribution is an intriguing problem, which might argue for the transfer of angular momentum by bars or spiral waves in the disk or unvirialised lumps in the halo. We will not digress into this issue since the goal of our analytical and N-body modeling is to explore the maximum effect of blowing out the exponential disks.

We have decided to make an alternative choice of the functional form of the initial cumulative distribution of the specific angular momentum of baryons,

$$\frac{M_b(< j)}{f_b M_{\rm vir}} = 1-\exp\left(-\frac{j^n}{j_0^n}\right), \qquad n \equiv \frac{6-2\gamma}{4-\gamma}, \quad (5)$$

where $1.33 \geq n \geq 1.2$ for a general cusp slope $1 \leq \gamma \leq 1.5$ of the initial halo, and $j_0$ is a characteristic specific angular momentum, related to the median angular momentum by $j_{\rm median} \equiv j_0(\ln 2)^{1/n}$. This parametrization can describe the angular momentum profile of observed disks fairly well (cf Fig. 2), albeit with significant scatter. It also creates an approximately exponential disk after adiabatic contraction. This can be understood roughly since $j = r_j v_j \propto r_j$ in a model with a nearly flat rotation curve, so that equation (5) corresponds to an almost exponential distribution in radius $r_j$. Also, our angular momentum profile reproduces the asymptotic profile $M_b \propto j^{4/3} \propto r_j^2$ near the center, as expected for the exponential disk embedded in a Hernquist halo with $\gamma = 1$ and $n = 4/3$. The characteristic specific angular momentum $j_0$ is determined by the integrated total angular momentum $J$ of the initial halo,

$$\int_0^\infty dx_j x_j \frac{d\left[1-\exp\left(-x_j^n\right)\right]}{dx_j} = \frac{J}{M_{\rm vir} j_0} = \frac{\lambda G M_{\rm vir}^{3/2}|E|^{-1/2}}{j_0}, (6)$$

where the l.h.s. can be reduced to the gamma function, $\Gamma(1+1/n)$. Since the baryons have initially the same distribution as dark matter, the total energy of the system is

$$|E| = (1-f_b)^{-2}\int_0^\infty dr \frac{dM_{dm}}{dr}\frac{GM_{dm}}{2r} = \frac{GM_{\rm vir}^2}{4(5-2\gamma)r_s}, \quad (7)$$

and we can express $j_0$ in terms of the $\lambda$ parameter,

$$j_0 = \frac{\lambda\sqrt{GM_{\rm vir} r_s}}{\xi}, \qquad \xi \equiv \Gamma(1+1/n)/\sqrt{4(5-2\gamma)}. \quad (8)$$

At small radii the initial mass distribution of dark matter is

$$M_{dm} \to (1-f_b)M_{\rm vir}\left(\frac{r_i}{r_s}\right)^{3-\gamma}, \qquad r_i \to 0, \quad (9)$$

and the initial specific angular momentum

$$j \propto \sqrt{M_{dm} r_i} \propto r_i^{\frac{4-\gamma}{2}} \propto M_{dm}^{\frac{4-\gamma}{6-2\gamma}}. \quad (10)$$

So with our choice of $n$, the asymptotic angular momentum distribution of the baryons scales the same way as that of the dark matter:

$$M_{dm} \propto M_b \propto j^n, \qquad j \to 0. \quad (11)$$

It follows then that the mass profiles of the baryons and dark matter are similar before and after the contraction,

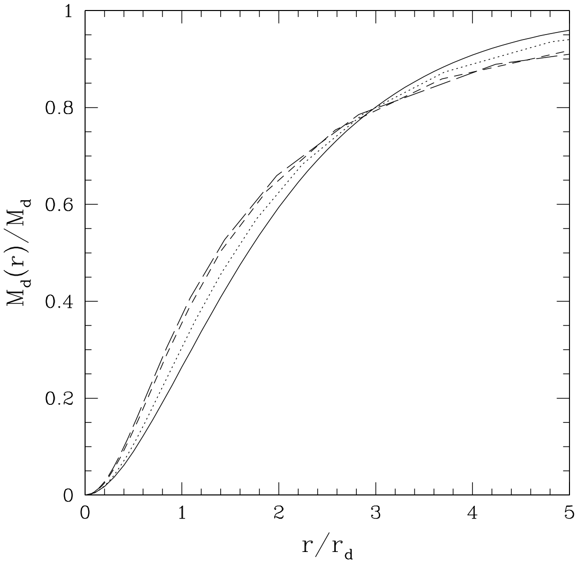

**Figure 3.** Baryon mass profile according to our angular momentum prescription, in comparison with the exponential disk profile (solid line; cf. eq. 4). The radii are normalized to the scale length $r_d$ computed numerically for three cases: $\lambda = 0.05$ (dots), $\lambda = 0.01$ (short dashes), $\lambda = 0.0025$ (long dashes).

$$M_b \propto M_{dm} \propto r_i^{3-\gamma} \propto j^n \propto r_j^{3-\gamma}, \tag{12}$$

where

$$r_j \propto j^{\frac{2}{4-\gamma}} \propto r_i \tag{13}$$

is the post-contraction radius. The contraction factor is finite at small radii, and the cusp slope of the dark matter does not change. To summarize, at small radii after the contraction we have

$$\begin{aligned} M_{dm} &\rightarrow (1-f_b)M_{\rm vir}\left(\frac{Cr_j}{r_s}\right)^{3-\gamma}, & (14)\\ M_b &\rightarrow \xi^n\lambda^{-n}f_b M_{\rm vir}\left(\frac{Cr_j}{r_s}\right)^{3-\gamma}, & (15)\\ r_j &\rightarrow C^{-1}r_i, & (16)\end{aligned}$$

where

$$C \equiv 1 + (\xi^n\lambda^{-n} - 1)f_b. \tag{17}$$

At a given radius $r_j$, the enclosed dark mass and density are enhanced by a factor $C^{3-\gamma}$. For an initial Hernquist halo, $\gamma = 1$, $n = 4/3$, and $\xi = 0.265$. For the disk parameters $f_b = 0.13$, $\lambda = 0.05 - 0.01$, the inner dark matter density is enhanced by a factor $C^2 = 4 - 160$.

It is interesting to note that the model with $\gamma = 1$ produces an asymptotic mass distribution at small radii, $M_b \propto r_j^2$, similar to that of an exponential disk (cf eq. 4). Figure 3 shows the computed mass profiles of baryons for a family of models with different $\lambda_b$. Our analytical models reproduce exponential profiles at 10% level within $0.5 - 5$ scale lengths. The difference in the disk potential is even less and therefore the adiabatic contraction of dark matter is very similar. For all three models, the dark matter profiles computed with the two methods are essentially indistinguishable between $10^{-3}$ and $10\,r_s$.

### 3.2 Analytical models of slow wind and fast wind

The expulsion of gas can be worked out analytically in two limiting cases: the adiabatic and instantaneous regimes. We shall refer to these as the slow wind and the fast wind, respectively. The outflow can play a significant role in massive galaxies as well as in dwarf galaxies. Our analytical description is similar to that used in estimating the maximum wind-induced expansion of the dark halo of the Milky Way (Zhao 2002).

To gain more analytical insight, we first consider the slow wind. In this case, a circular orbit of radius $r_j$ expands to a circular orbit of radius $r_f$ while conserving the specific angular momentum $\sqrt{GM(r)r}$. So the expansion factor is inversely proportional to the combined enclosed mass of baryons and dark matter, i.e.,

$$\left.\frac{r_f}{r_j}\right|_{\rm slow} = \frac{M_{dm}(r_j) + M_b(r_j)}{M_{dm}(r_j) + M_b(r_j) - M_w(r_j)} \tag{18}$$

where $M_b(r_j)$ and $M_{dm}(r_j)$ are the baryon and dark matter masses within radius $r_j$, and $M_w(r_j)$ is the amount of baryons "gone with the wind". Alternatively, we can write

$$r_f|_{\rm slow} = \frac{r_j}{1 - f_w(r_j)}, \tag{19}$$

where

$$f_w(r_j) \equiv \frac{M_w(r_j)}{M_{dm}(r_j) + M_b(r_j)}, \tag{20}$$

measures the blown-away mass as a fraction of the dynamical mass. The expansion factor $r_f/r_j$ is larger in the inner region where the baryons are concentrated and is minimal at the virial radius, where we have only a modest change, since

$$f_w(r_{\rm vir}) = \delta f_b \lesssim 0.1, \tag{21}$$

where $0 \le \delta \le 1$ is the total fraction of baryons blown away.

Although we do not know of any close form for the effect of fast wind, we could modify equation (19) for slow wind to mimic the effects of wind of arbitrary strength. We suggest the following simple formula

$$r_f = \frac{r_f|_{\rm slow}}{\left[1 - f_w(r_j)\right]^{\frac{k}{4}}\left(1 - 2^k\delta f_b\right)^{\frac{k}{4}}}, \qquad 0 \le k \le 1, \tag{22}$$

where $k$ is a tunable parameter to model the rapidity of the wind. For example, slow wind is a special case with $k = 0$ (cf eq. 19). The instantaneous wind is modeled with $k = 1$, following the rule of thumb that a system becomes unbound if it loses half of the mass instantaneously. To verify this, we substitute $k = 1$ and $f_w(r_{\rm vir}) \rightarrow 1/2$ in equation (22) and find that the r.h.s. factor $1 - 2^k\delta f_b = 1 - 2f_w(r_{\rm vir}) \rightarrow 0$, hence $r_f \rightarrow \infty$. For the winds of moderate speed with $k < 1$ and moderate mass-loss with $f_w(r_{\rm vir}) < 2^{-k}$, the system remains bound and expands by a certain factor at large radii. At small radii, where the baryons always dominate with $f_w(r_j) \rightarrow 1$, the particles may not necessarily escape to infinity because they slow down when they cross the orbits of outer particles. As we will show in §4, this empirical parametrization turns out to approximate well the results of numerical simulations.

To work out the properties of the model at very small radii, we substitute equations (14-17) in equation (20) and obtain

$$f_w \to \xi^n \lambda^{-n} \delta\, C^{-1} f_b. \tag{23}$$

Substituting equations (16,23) in equation (22), we find that in the center the final post-wind radius $r_f$ is related to the initial pre-contraction radius $r_i$ by

$$F \equiv \frac{r_f}{r_i} = \frac{\left[1 + (\xi^n \lambda^{-n} - 1) f_b\right]^{\frac{k}{4}}}{\left[1 + (\xi^n \lambda^{-n}(1-\delta) - 1) f_b\right]^{1+\frac{k}{4}} \left(1 - 2^k \delta f_b\right)^{\frac{k}{4}}}. \tag{24}$$

The slope of the cusp remains the same. By comparing the dark matter mass within a given radius, we find that the density is reduced by a factor $F^{3-\gamma}$.

### 3.3 Maximum effect on the final halo density

The strongest effect on the halo is achieved in the limit of complete removal of the baryonic disk, i.e., $\delta \to 1$. In this case we have for all radii

$$r_f = \frac{r_i}{(1-f_b)} \left[\frac{1 + M_b/M_{dm}}{1 - 2^k f_b}\right]^{\frac{k}{4}}, \qquad \delta \to 1. \tag{25}$$

Interestingly, if the disk forms slowly and is removed slowly as well (i.e., with $k = 0$), the halo expands slightly by a constant factor

$$\frac{r_f}{r_i} = (1 - f_b)^{-1} = const, \tag{26}$$

as expected from adiabatic invariance. The result is the same if all the baryons were removed from the initial halo distribution without going through the phase of disk formation.

The effect is maximized when a very dense disk ($\lambda \ll 0.05$) is removed instantaneously ($k = 1$). If the initial halo is a Hernquist model (i.e., $\gamma = 1$, $n = \frac{4}{3}$, and $\xi = 0.265$), then close to the center the halo will expand by a factor (cf eq. 24)

$$F \sim \frac{1}{1-f_b} \left[\frac{f_b}{(1-f_b)(1-2f_b)}\right]^{\frac{1}{4}} \left(\frac{0.265}{\lambda}\right)^{\frac{1}{3}} \sim \left(\frac{0.15}{\lambda}\right)^{\frac{1}{3}}, \tag{27}$$

relative to the original halo model. Here we assume a universal baryon fraction $f_b = 0.13$ to make a massive disk. To summarize, the density of the innermost dark matter can drop at most by a factor $F^2 = 2 - 6$ for $\lambda = 0.05 - 0.01$.

## 4 SPHERICAL SHELL SIMULATIONS

To confirm the analytical results, we compute the dynamics of dark matter using the spherical shell method of Gnedin & Ostriker (1999). The algorithm, originally due to L. Spitzer and collaborators, utilizes spherical geometry to achieve high resolution in the center. Dark matter particles are distributed on concentric spherical shells at radii $r_k$ with the mean energy $E_k$ and angular momentum $j_k$. Shells move in the radial direction with the velocity $v_{r,k}$ and can freely cross each other.

We have extended the code of Gnedin & Ostriker (1999) by including variable shell masses, $m_k$, and improving the corrections for shell crossing. The code solves the equations of motion using the first integral, $C_k$:

$$v_{r,k}^2 + \frac{j_k^2}{r_k^2} - \frac{2GM(r_k)}{r_k} = C_k, \tag{28}$$

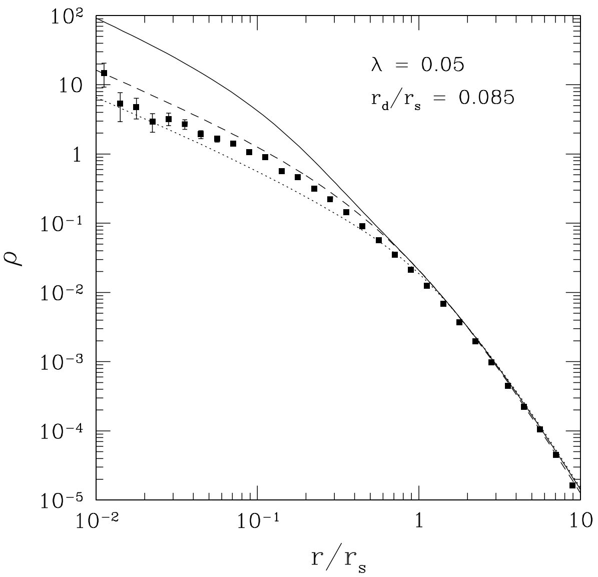

**Figure 4.** Dark matter density profiles for Model A ($\lambda = 0.05$, $f_b = 0.13$, $\delta = 1$) before and after the gas removal. Dashed line is the initial Hernquist model, solid line is the halo profile after the adiabatic contraction. Symbols show a new equilibrium profile after the removal of the baryonic disk, computed with $10^5$ spherical shells. Errorbars are the sampling uncertainty. Dotted line is the analytical prediction, eq. (25).

where $M(r_k)$ is the mass enclosed within shell $k$, including a half of its own mass (accounting for the shell self-gravity):

$$M(r_k) = \sum_{j=1}^{k-1} m_j + \frac{m_k}{2}, \tag{29}$$

if the shells are ordered in radius. The integrals $C_k$ determine the turn-around points where the direction of the shell's velocity is reversed. At each time step, the code finds the locations of all shell crossings and adjusts the integrals $C_k$ according to the changed enclosed mass. Because of such corrections, two-body interactions are effectively reduced and there is no need for force softening. As a result, the central region of the system can be probed with very high accuracy.

In order to investigate the effect of angular momentum loss, we have run three models: Model A with the mean value of $\lambda = 0.05$, and Models B and C where $\lambda$ deviates from its mean by $3\,\sigma_\lambda$ ($\lambda = 0.01$, Model B) and $6\,\sigma_\lambda$ ($\lambda = 0.0025$, Model C).

We use the units $G = 1$, $M_{\rm vir} = 1$, $r_s = 1$, and therefore the results can be scaled to any halo parameters. Each model is run with $N = 10^4$, $4 \times 10^4$, and $10^5$ shells to check numerical convergence. After the disk is removed, the models are run for 40 half-mass dynamical times ($t_{\rm dyn} = 8$ in code units) to ensure that a new dynamical equilibrium is achieved.

Figure 4 shows the initial halo profile and the new equilibrium distribution after the instantaneous removal of the whole disk in Model A. The scale length of the disk, $r_d = 0.085\, r_s$, is already a small fraction of the scale radius of the halo. As expected, there is no change in the profile outside the cusp, at $r > r_s$. But even inside the scale radius,

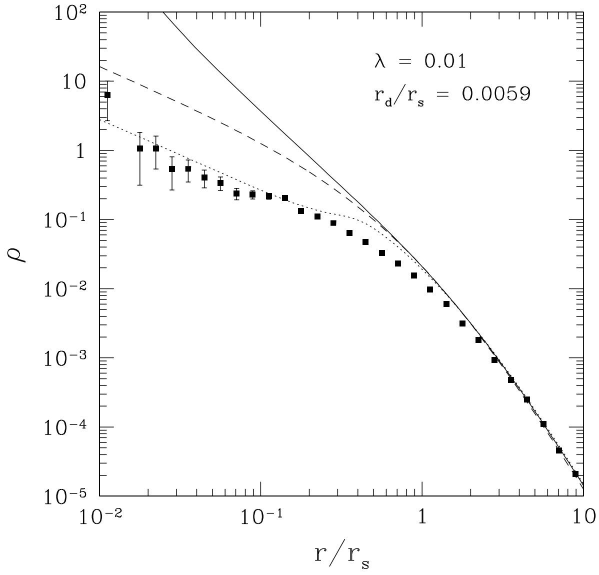

**Figure 5.** Density profiles for Model B ($\lambda = 0.01$). Lines are as in Figure 4.

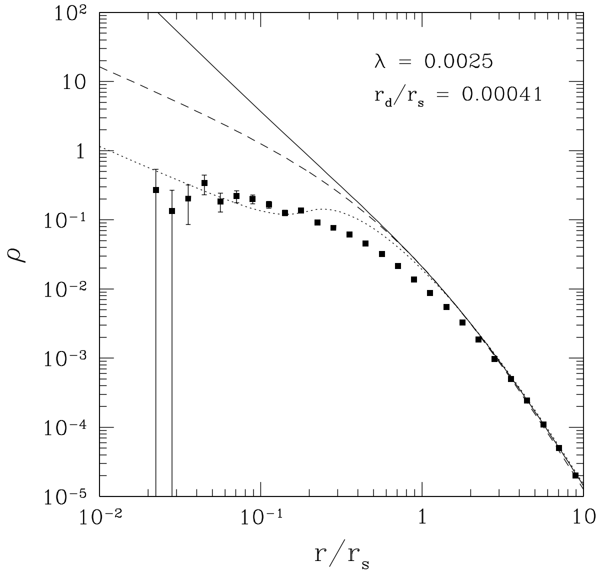

**Figure 6.** Density profiles for Model C ($\lambda = 0.0025$). Lines are as in Figure 4.

the new profile is fairly close to the initial model prior to adiabatic contraction. The central density is affected at most by a factor of 2, in agreement with the analytical prediction (eq. 27).

Figure 5 shows the density profile for Model B. The effect is stronger but there is still no indication of a core forming instead of the cusp. The asymptotic solution increases towards the center as $r^{-1}$ and describes the numerical result reasonably well.

Finally, Model C may have achieved a central core (Figure 6). The inner profile can be fitted with an approximate isothermal sphere, $\rho \propto (r^2 + r_c^2)^{-1}$, where $r_c \approx 0.2\, r_s$. This core radius is significantly larger than the tiny initial scale-length of the disk, $r_d = 0.00041\, r_s$. However, it seems that the energy input has already saturated in Model C (the change in the binding energy is similar to Model B) and further contraction of the disk would not lead to a larger core.

After the disk is removed, the dark matter particles with a large enough kinetic energy become unbound. At the end of the simulation, the halo in Model A loses 6.5% of its mass, while halos B and C lose 14% and 16%, respectively. (About half of those particles become unbound during the subsequent evolution of the halo potential towards a new equilibrium.) However, as the disk is made progressively more compact, the heating caused by the disk removal is shared by a small number of particles in the center. They reach very high velocities and leave the system, whereas most of the particles remain unaffected. In the limit of an infinitely small disk, the final equilibrium profile would still be close to our extreme Model C.

### 4.1 Artificial numerical effects

As any N-body simulation, our models are affected to some extent by the artificial numerical relaxation. This relaxation arises from the small-scale particle encounters and from the Poisson potential fluctuations due to discreteness (Hernquist & Barnes 1990; Weinberg 1993). Even though the shell-crossing corrections in our code remove the small-scale errors, the large-scale fluctuation modes are unavoidable.

The relaxation time over which the particle energy changes by the order itself can be estimated at the half-mass radius of the system, $R_h$, from (Spitzer & Hart 1971):

$$t_r \approx 0.14\, \frac{N}{\ln \Lambda} \left( \frac{R_h^3}{GM} \right)^{1/2}, \qquad (30)$$

where $\ln \Lambda \sim \ln N$ is the usual Coulomb logarithm. In the code units, $G = 1$, $M = 1$, and with $R_h \approx r_s = 1$, we have

$$t_r \sim 0.1\, \frac{N}{\ln N}. \qquad (31)$$

This expression can be compared with the relaxation rate (inverse of the relaxation time) derived by Weinberg (1993). His Fig. 3 expresses $t_r$ as a function of the system size divided by the Jeans length. For a virialised Hernquist model, this ratio can be 0.6−0.8 and reading of the plot gives $t_r \sim 25 - 50$. It agrees with equation (31) for the particle number $N = 4000$ used by Weinberg (1993).

Thus, the large-scale potential fluctuations can only be reduced by increasing the number of particles in the simulation. We estimate that our results with $N = 10^5$ shells are unaffected by the relaxation at the scale radius $r_s$ for $t \ll t_r \approx 800 \approx 100\, t_{\rm dyn}$. The rate of relaxation does not increase much in the inner parts, because it is dominated by the global modes and not by local encounters.

Another numerical effect, which is more important for the inner shells than the outer shells, is the kinematic error due to a finite time step. We chose $\Delta t = t_{\rm dyn}/N$, so that each shell crosses on average one other shell. Since the density at $r < r_s$ goes approximately as $\rho(r) \propto r^{-1}$, the orbital period of a shell $t_{\rm orb}(r) \approx t_{\rm dyn}\, (r/r_s)^{1/2}$. This shows that if 10 time steps are necessary to properly resolve an orbit, our results are valid down to a tiny radius $r \sim (10/N)^2\, r_s \sim 10^{-8}\, r_s$.

### 4.2 Comparison with previous work

Navarro, Eke & Frenk (1996) studied the effect of instantaneous disk removal using a three-dimensional N-body code. They also used a Hernquist model for the initial dark matter profile and imposed an external potential of the exponential disk. Instead of analytically calculating the adiabatic contraction, they let the dark matter halo to adjust dynamically to the disk potential. Then, they removed the disk and studied the subsequent expansion of the halo. Navarro et al. found that the core did develop in the inner regions of all of their models. They fit a non-singular isothermal sphere to the inner 25% of the mass and found the core radii satisfying the following relation: $r_c = 0.11\,(M_d/r_d)^{1/2}\, r_s$, where $M_d$ is the mass of the disk in units of the halo mass (or $f_b/(1-f_b)$, in our notation).

The expansion effect that Navarro et al. find is much stronger than what our simulations or analytical modeling show. For example, their fit for the core radius would give for our Model C, $r_c \approx 2.1$, about ten times the value we find. In Models A and B the core radii should also have been easily detectable, according to the fit.

We identify two possible reasons for the disagreement, force resolution and numerical relaxation effects. Firstly, a force softening at 0.03 $r_s$, used by Navarro, Eke & Frenk (1996), could prevent an accurate calculation of the dynamics of inner particles, especially in cases of very small disks. This would naturally cause a development of a core in the particle distribution, although the core radii found by Navarro et al. are larger than the softening length. Secondly, numerical effects might be important, as their simulations use only $N = 10^4$ particles. The relaxation time, $t_r \sim 100$ time units, is 4 to 6 times shorter than the duration of their experiments. Even though Navarro et al. demonstrate that the numerical profile before the disk removal is stable, it may be more susceptible to the relaxation afterwards, when a smaller number of particles is left in the center. This may also lead to a simple statistical undersampling of the density distribution, posing as a 'core'.

It is likely that the difference in the results is not related to the geometry, 1D vs 3D simulations. In our one-dimensional models, all shells conserve their initial angular momentum and do not experience any non-radial perturbations. But since the dark matter halo is not centrifugally supported, precise conservation of angular momentum should not seriously affect the dynamics. Also, the remaining stellar distribution in dwarf spheroidal galaxies is observed to be roughly spherical, so we can expect the dark matter halo to be spherical as well, lending support to our 1D models. Finally, we have checked that our different implementations of the adiabatic contraction gave almost identical initial conditions and therefore cannot be responsible for the disagreement.

Note, that our simulations achieve much higher resolution, with ten times more particles and no force softening in the center. But the statistical error-bars in Figure 6, inversely proportional to the square root of the number of particles in the bin, show that even our models cannot probe regions smaller than $0.01 - 0.03\, r_s$. At larger radii, except for the extreme model C, we do not find any significant flattening of the dark matter distribution.

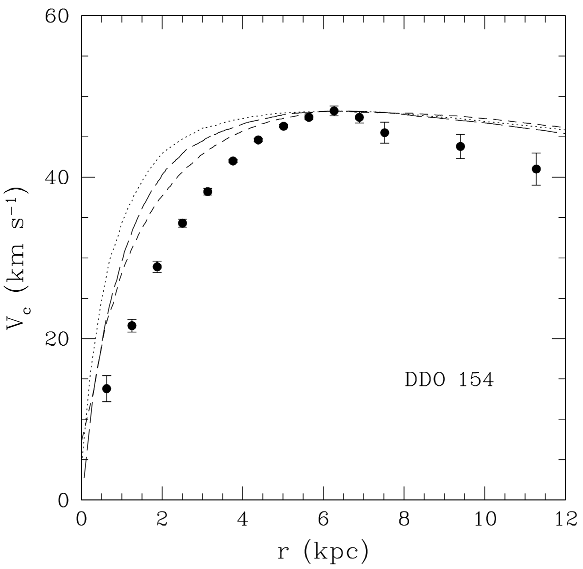

**Figure 7.** Rotation curve of DDO 154 from a high-resolution HI data (from Carignan & Purton 1998) compared with the final circular velocities of Models A (dots), B (short dashes), and C (long dashes). The simulated rotation curves are normalized to pass through the maximum of the observed one, with no formal fitting attempted.

Any realistic modeling of stellar feedback would have an even weaker effect. Lia, Carraro & Salucci (2000), using a more complex tree-SPH simulation of star formation in a dwarf galaxy, find that the central cusp remains intact.

### 4.3 Application to DDO 154

Our results demonstrate that stellar feedback is insufficient to reduce the central dark matter density. We illustrate this point for a prototypical low surface brightness galaxy DDO 154. Figure 7 shows the observed rotation curve of DDO 154, which peaks at 48 km s$^{-1}$. As this is perhaps the most robustly determined quantity, we normalize the simulation results to have the same value and location of the circular velocity. The simulated curves correspond to the final equilibrium density profiles of Models A, B, and C. They are clearly more concentrated than allowed by the data.

In addition, the scale radii of the initial halo in Figure 7 increase as the effect of feedback gets weaker (corresponding to the larger disk). For Model C $r_s = 2.9$ kpc, but for the less perturbed models B and A it is $r_s = 3.6$ and 5.6 kpc, respectively. The virial halo mass is about the same, around $1.3 \times 10^{10}\, M_{\odot}$. This mass is lower than the best-fitting value ($\sim 3 \times 10^{10}\, M_{\odot}$) from van den Bosch et al. (2000), and yet the resulting rotation curve is well above observations.

Note, that we do not attempt any accurate fitting of the rotation curve. The beam-smearing effects are likely to be unimportant (beam size is less than 1 kpc; van den Bosch et al. 2000), and therefore the small error-bars in the inner parts place very strong constraints on the allowed dark matter profiles. Gelato & Sommer-Larsen (1999) used a set of N-body simulations to address this issue. They selected three halos with $M \sim 10^{10}\,M_\odot$ at $z = 0$ from a random realization of a $4\,h^{-1}$ Mpc box with the SCDM power spectrum. Varying the amount of gas and the concentration of the dark matter halo, Gelato & Sommer-Larsen (1999) could find a satisfactory fit to the inner rotation curve of DDO 154 only (1) if the present disk contained 3 times more gas than is observed and (2) if the halo had a low concentration, $r_{\rm vir}/r_s = 4$. However, none of their models could fit simultaneously the inner and outer parts of the rotation curve.

## 5 SUMMARY

We have explored the effect of maximum feedback on the central density of dark matter halos of the gas-rich dwarfs, combining analytical limits with numerical simulations. The expansion of dark matter after the removal of the entire disk is controlled by the mass and compactness of the disk. For a wide range of the baryon angular momenta, we find the effect to be modest, at most a factor of 2 to 6 reduction in the central halo density. This is hardly enough to bring the models into agreement with the observed solid-body rotation curves, as we demonstrate for the case of DDO 154.

We conclude that the slowly rising rotation curves are likely to be a genuine problem of CDM models. It might be necessary to consider other possible solutions, such as the effect of merging of massive black holes or an unusual property of dark matter particles.

### Acknowledgements

We would like to thank Martin Rees for discussions, and Frank van den Bosch for comments and for making available the data used for generating Fig. 2.

## REFERENCES

Bahcall N. A., Ostriker J. P., Perlmutter S., Steinhardt P. J., 1999, Science, 284, 1481
Barnes J., Efstathiou G., 1987, ApJ, 319, 575
Blumenthal G. R., Faber S. F., Flores R., Primack J. R., 1986, ApJ, 301, 27
Bode P., Ostriker J. P., Turok N., 2001, `astro-ph/0010389`
Bullock J. S. et al., 2001a, MNRAS, 321, 559
Bullock J. S., Dekel A., Kolatt T. S., Kravtsov A. V., Klypin A. A., Porciani C., Primack J. R., 2001b, ApJ, 555, 240
Carignan C., Purton C., 1998, ApJ, 506, 125
Dalcanton J. J., Spergel D. N., Summers F. J., 1997, ApJ, 482, 659
de Blok W. J. G., McGaugh S. S., Bosma A., Rubin V. C., 2001, ApJ, 552, L23
Dekel A., Silk J., 1986, ApJ, 303, 39
Efstathiou G., Frenk C. S., White S. D. M., Davis M., 1988, MNRAS, 235, 715
Flores R., Primack J. R., Blumenthal G. R., Faber S. M., 1993, ApJ, 412, 443
Gelato S., Sommer-Larsen J., 1999, MNRAS, 303, 321
Gnedin O. Y., Ostriker J. P., 1999, ApJ, 513, 626
Hernquist L., 1990, ApJ, 356, 359
Hernquist L., Barnes J. E., 1990, ApJ, 349, 562
Klypin A., Kravtsov A. V., Valenzuela O., Prada F., 1999, ApJ, 522, 82
Lia C., Carraro G., Salucci P., 2000, A&A, 360, 76
Mateo M., 1998, ARA&A, 36, 435
Mo H. J., Mao S., White S. D. M., 1998, MNRAS, 295, 319
Moore B., Ghigna S., Governato F., Lake G., Quinn T., Stadel J., Tozzi, P. 1999a, ApJ, 524, L19
Moore B., Quinn T., Governato F., Stadel J., Lake G., 1999b, MNRAS, 310, 1147
Navarro J. F., Benz W., 1991, ApJ, 380, 320
Navarro J. F., Eke V. R., Frenk C. S., 1996, MNRAS, 283, L72
Navarro J. F., Frenk C. S., White S. D. M., 1997, ApJ, 490, 493
Navarro J. F., Steinmetz M., 2000, ApJ, 538, 477
Spergel D. N., Steinhardt P. J., 2000, Phys. Rev. Lett., 84, 3760
Spitzer L. Jr, Hart M. H., 1971, ApJ, 164, 399
Tyson J. A., Kochanski G. P., dell'Antonio I. P., 1998, ApJ, 498, L107
van den Bosch F. C., Robertson B. E., Dalcanton J. J., de Blok W. J. G., 2000, AJ, 119, 1579
van den Bosch F. C., Burkert A., Swaters R. A., 2001, MNRAS, 326, 1205
Weinberg M. D., 1993, ApJ, 410, 543
Zhao H.S. 1996, MNRAS, 278, 488
Zhao H.S. 2002, MNRAS, submitted